ARCHIVIO ISTITUZIONALE
DELLA RICERCA

Alma Mater Studiorum Università di Bologna
Archivio istituzionale della ricerca

Metabolic Tumor Volume Assessed by 18F FDG-PET CT Scan as a Predictive Biomarker for Immune Checkpoint Blockers in Advanced NSCLC and Its Biological Correlates

This is the final peer-reviewed author's accepted manuscript (postprint) of the following publication:

Published Version:
Dall'Olio, F.G., Zrafi, W., Roelants, V., Ambrosini, V., Fourquet, A., Mitea, C., et al. (2025). Metabolic Tumor Volume Assessed by 18F FDG-PET CT Scan as a Predictive Biomarker for Immune Checkpoint Blockers in Advanced NSCLC and Its Biological Correlates. CLINICAL CANCER RESEARCH, 31(2), 352-364 [10.1158/1078-0432.CCR-24-1993].

Availability:
This version is available at: https://hdl.handle.net/11585/1013430 since: 2025-04-01

Published:

DOI: http://doi.org/10.1158/1078-0432.CCR-24-1993

Terms of use:

Some rights reserved. The terms and conditions for the reuse of this version of the manuscript are specified in the publishing policy. For all terms of use and more information see the publisher's website.

This item was downloaded from IRIS Università di Bologna (https://cris.unibo.it/).
When citing, please refer to the published version.

(Article begins on next page)

09 November 2026

Metabolic tumor volume assessed by 18F FDG - PET CT scan as a predictive biomarker for immune checkpoint blockers in advanced NSCLC and its biological correlates.

Authors

Filippo G. Dall'Olio[1,2], Wael Zrafi[3], Veronique Roelants[4], Valentina Ambrosini[5,6], Aloyse Fourquet[7], Cristina Mitea[8,9], Francesco Passiglia[10], Matteo Bauckneht[11,12] Gerald Bonardel[13], Nicole Conci[14], Jose Carlos Benitez[15], Vincenzo Arena[16], Céline Namour [17], Marie Naigeon[18,19,20], Isabelle Monnet[21], Kristi Beshiri[22], Delphine Hoton[23], Safiye Dursun[24], François Xavier Danlos[25,19], Giulia Argalia[5], Mihaela Aldea[1,19], Guido Rovera[16], Lisa Derosa[25,26,27], Valerio Iebba[28], Hester A. Gietema[9,29], Valerie Gounant[17], Valérie Lacroix[30], Jordi Remon[1], Daniel Gautheret[3], Nathalie Chaput[18,20], Bastien Job[3], Patricia L. Kannouche[31], Monica Velasco-Nuño[32], Laurence Zitvogel [25,26,27,33], Eugenia Cella[34], José Reinaldo Chícharo de Freitas[35], Damien Vasseur[36], Mohamed Aymen Bettaieb[37], Marco Tagliamento[34,1], Lizza Hendriks[24], Antoine Italiano[22], David Planchard[1,19], Aurelien Marabelle[22], Fabrice Barlesi[1,19], Silvia Novello[10], Desiree De Andreis[37], Frank Aboubakar Nana[38], Andrea Ardizzoni[14], Gerard Zalcman[17], Camilo Garcia[37*], Benjamin Besse[1, 18*].

Affiliations

1) Cancer Medicine Department, Gustave Roussy, Villejuif, France.
2) *METSY laboratory Metabolic and systemic aspects of oncogenesis for new therapeutic approaches* - UMR 9018 CNRS and Université Paris-Saclay
3) Department of Biostatistics and Bioinformatics, Gustave Roussy, Villejuif, France.
4) Nuclear Medicine Department, Cliniques Universitaires Saint-Luc, Brussels, Belgium.
5) Nuclear Medicine, Alma Mater Studiorum University of Bologna
6) Nuclear Medicine, IRCCS Azienda Ospedaliero-Universitaria di Bologna

7) Department of Nuclear Medicine, Hôpital Bichat-Claude Bernard, AP-HP.Nord, Univesité Paris Cité, Paris, France.
8) Department of Radiology and Nuclear Medicine, Maastricht University Medical Centre, Maastricht, The Netherlands.
9) GROW-School for Oncology and Reproduction, Maastricht University Medical Center, Maastricht, the Netherlands.
10) Department of Oncology, University of Turin, San Luigi Hospital, Orbassano (TO), Italy.
11) Nuclear Medicine Unit, IRCCS Ospedale Policlinico San Martino, Genova, and Department of Health Sciences (DISSAL), University of Genoa, Genoa, Italy.
12) IRCCS Ospedale Policlinico San Martino, Genova, Italy.
13) Department of Nuclear Medicine, Centre Cardiologique du Nord, Saint-Denis, France.
14) Medical Oncology, IRCCS Azienda Ospedaliero-Universitaria di Bologna, Italy
15) Medical Oncology Intercenter Unit. Regional and Virgen de la Victoria University Hospitals. IBIMA. Málaga. Spain. Research Biomedical Institute of Malaga (IBIMA); Malaga, Spain.
16) Nuclear Medicine Division, Department of Medical Sciences, University of Turin, Turin, Italy.
17) Thoracic Oncology Department-Early Phases Unit CIC-1425 Inserm, Institut du Cancer AP-HP.Nord, Hôpital Bichat-Claude Bernard, 46 Rue Henri Huchard, 75018 Paris, France.
18) Laboratoire d'immunomonitoring en Oncologie, INSERM US23, CNRS UMS 3655, Gustave Roussy, Villejuif, France.
19) Faculté de médecine, Université Paris-Saclay, Le Kremlin-Bicêtre, France
20) Faculté de pharmacie, Université Paris-Saclay, Orsay, France
21) Pneumology Department, Intercommunal Hospital of Creteil (CHI), Creteil, France.
22) Département d'Innovation Thérapeutique et d'Essais Précoces (DITEP), Gustave Roussy, Université Paris Saclay, Villejuif, France.
23) Department of Pathology, Cliniques universitaires Saint-Luc, Brussels, Belgium.
24) Department of Pulmonary Diseases, GROW-School for Oncology and Reproduction, Maastricht University Medical Center+, Maastricht, the Netherlands.
25) Gustave Roussy, Villejuif, France.
26) Institut National de la Santé Et de la Recherche Médicale (INSERM) U1015, Equipe Labellisée - Ligue Nationale contre le Cancer, Villejuif, France.
27) Faculté de Médecine, Université Paris-Saclay, Kremlin-Bicetre, France.
28) Department of Medical, Surgical and Health Sciences, University of Trieste, Trieste, Italy.
29) Maastricht University Medical Centre, Maastricht University, Maastricht, the Netherlands.
30) Department of Cardiovascular and Thoracic Surgery, IREC, Cliniques Universitaires Saint-Luc, Brussels, Belgium.
31) UMR9019-CNRS, IGC Université Paris Saclay, Gustave Roussy, Villejuif, France
32) Department of Nuclear Medicine Hospital HM Nou Delfos, HM Hospitales, Barcelona, Spain.
33) Center of Clinical Investigations BIOTHERIS, INSERM CIC1428, Villejuif, France.
34) Dipartimento di Medicina Interna e Specialità Mediche (DiMI), Università degli Studi di Genova, 16132 Genoa, Italy.

35) Nuclear Medicine Unit, CIMES-FGUMA, Málaga, Spain.
36) Department of Medical Biology and Pathology, Gustave Roussy, Villejuif, France.
37) Nuclear Medicine Department, Gustave Roussy, Villejuif, France.
38) Département de Pneumologie, Cliniques Universitaires St-Luc, Brussels, Belgium

* Contributed equally as last author

Running title

Metabolic tumor volume and immunotherapy in NSCLC

Correspondence to: Camilo Garcia, Gustave Roussy, 114 Rue Edouard Vaillant, 94805 Villejuif, France
Email address: Camilo.GARCIA@gustaveroussy.fr

Conflict of interests statement

Valentina Ambrosini reported Speaker fees from ESMIT/ESMO/EANM, Cineca and AAA (in the last 5years). Member of: the Oncology and theranostic EANM committee, the ENETS advisory board, the ESMO faculty staff for NET, the scientific board of ITANET

Francesco Passiglia received speakers' and consultants' fee from Astra-Zeneca, BMS, Novartis, Roche, MSD, Amgen, Janssen, Sanofi, Beigene, Thermofisher Scientific;

Silvia Novello declared speaker bureau/advisor's fee from Boehringer Ingelheim, Roche, Merck Sharp, and Dohme, Amgen, Thermo Fisher Scientifics, Eli Lilly, GlaxoSmithKline, Merck, AstraZeneca, Janssen, Novartis, Takeda, Bayer, Pfizer.

Jordi Remon has acted as an adviser for Bayer, BMS, Boehringer Ingelheim, GenMab, Janssen, MSD and Takeda; has received speaker fees from Janssen and Pfizer; has received honoraria from MSD; and has received travel fees from AstraZeneca, BMS, OSE Immunotherapeutics and Roche.

Lizza Hendriks has reported non-financial COIs Ad board: Amgen, Boehringer Ingelheim, Lilly, Novartis, Pfizer, Takeda, Merck, Janssen, MSD, Anheart. speaker educationals: AstraZeneca, Bayer, Lilly, MSD, high5oncology, Takeda, Janssen, GSK, Sanofi, PFizer (self) webinars and educationals Medtalks, VJOncology, Benecke, Medimix

(self) member dutch guideline committees NSCLC, brain metastases and leptomeningeal metastases. and non-financial: chair EORTC LCG NSCLC systemic therapy, secretary NVALT studies foundation, vice-chair scientific committee Dutch Thoracic Group, as well as member ESMO SCLC guideline and lead other ESMO metastatic NSCLC Guidelines
(all to institution) Research funding: Roche, AstraZeneca, Boehringer Ingelheim, Takeda, Merck, Pfizer, Novartis. Gilead under negotiation (all to institution)

Marco Tagliamento: Medical writing: Amgen, MDS; Travel, accommodation: Eli Lilly

Fabrice Barlesi : Consulting or Advisory Role: Roche/Genentech (Inst), Novartis (Inst), Bristol Myers Squibb (Inst), AstraZeneca/MedImmune (Inst), Boehringer Ingelheim (Inst), Lilly (Inst), Merck Serono (Inst), MSD Oncology (Inst), Takeda (Inst), Bayer (Inst), Amgen (Inst), Eisai Europe (Inst), Sanofi (Inst), Mirati Therapeutics (Inst) Research Funding: Roche/Genentech (Inst), AstraZeneca/MedImmune (Inst), Bristol Myers Squibb (Inst), Pierre Fabre (Inst), AbbVie (Inst), Amgen (Inst), Bayer (Inst), Boehringer Ingelheim (Inst), Eisai (Inst), Lilly (Inst), Ipsen (Inst), Innate Pharma (Inst), Novartis (Inst), Merck Serono (Inst), MSD Oncology (Inst), Pfizer (Inst), Sanofi/Aventis (Inst), Takeda (Inst) Travel, Accommodations, Expenses: Roche/Genentech

Andrea Ardizzoni : Honoraria: AZD, BMS, Lilly, MSD Oncology Consulting or Advisory Role: AZD, MSD Oncology, BMS, Lilly, Novartis, Takeda, Janssen Oncology, Sanofi Research Funding: Roche (Inst), AstraZeneca (Inst), Bristol Myers Squibb/Celgene (Inst)

David Planchard reported -Consulting, advisory role or lectures: AstraZeneca, Abbvie, Bristol-Myers Squibb, Boehringer Ingelheim, Celgene, Daiichi Sankyo, Eli Lilly, Merck, Novartis, Janssen, Pfizer, Roche, Pierre-fabre, Takeda, ArriVent, Mirati, Seagen. Clinical trials research as principal or co-investigator (Institutional financial interests): AstraZeneca, Bristol-Myers Squibb, Boehringer Ingelheim, Eli Lilly, Merck, Novartis, Pfizer, Roche, Medimmun, Sanofi-Aventis, Taiho Pharma, Novocure, Daiichi Sankyo, Abbvie, Janssen, Pierre-fabre, Takeda, ArriVent, Mirati, Seagen. Travel, Accommodations, Expenses: AstraZeneca, Roche, Novartis, Pfizer
Nathalie Chaput**:** Financial Interests, Personal, Advisory Board, Strong-Iopredi Scientific Advisory Board: AstraZeneca; Financial Interests, Institutional, Invited Speaker, Educational Session On Immune Cell Death: Servier; Financial Interests, Institutional, Expert Testimony, Expertise On Immune Cell Death Biomarkers: Servier; Financial Interests, Personal, Invited Speaker: Cytune Pharma; Financial Interests, Institutional, Research Grant, Research grant to identify immune biomarkers associated to clinical response in patients treated with agonistic mAbs: GSK; Financial Interests, Institutional, Research Grant, Preclinical studies in mice: GSK; Financial Interests, Institutional, Research Grant, Immune profiling of Head & Neck tumors: Sanofi.
Desiree De Andreis: speaker/consultant Novartis, AAA, EISAI, Immedica

Gerard Zalcman reports receiving grant support from Inventiva, Roche-France, and Takeda; personal fees from AstraZeneca, Bristol Myers Squibb, Da Volterra, Merck Sharp & Dohme, and Pfizer; and nonfinancial support from AbbVie and Inventiva.

Benjamin Besse**:** Financial Interests, Institutional, Funding: 4D Pharma, AbbVie, Amgen, Aptitude Health, AstraZeneca, BeiGene, Blueprint Medicines, Boehringer Ingelheim, Celgene, Cergentis, Cristal Therapeutics, Daiichi Sankyo, Eli Lilly, GSK, Janssen, Onxeo,

Ose Immunotherapeutics, Pfizer, Roche-Genentech, Sanofi, Takeda, Tolero Pharmaceuticals; Financial Interests, Institutional, Research Grant: Chugai Pharmaceutical, EISAI, Genzyme Corporation, Inivata, Ipsen, Turning Point Therapeutics.

Other authors did not report potential conflict of interest

Translational relevance

In our study we found that tMTV independently stratify advanced NSCLC patients treated with immunotherapy. Its utility goes beyond prognostication, allowing to select the best upfront strategy. Moreover, as the effect of tMTV seems to be mainly driven by a different, immune suppressive plasma proteomic profile, this further support the use of intensified combination regime with chemotherapy that, being associated with increased response rate, would potentially allow a reduction of plasma levels of certain cytokines that, in turn, could help restore the immune response against cancer. We also found a correlation between tMTV and genomic instability, while no correlation was found with other biomarker such as gut microbiota and T cell senescence.

ABSTRACT

Purpose:

This study aimed to explore metabolic tumor volume (tMTV) as assessed 18F-fluorodeoxyglucose positron emission tomography-computed tomography (18F-FDG-PET/CT), and understand its biological meaning in patients with NSCLC exposed to immune checkpoint blockers(ICBs).

Experimental Design:

In this study, patients with advanced NSCLC and a positive PET scan within 42 days of first line treatment were enrolled in 11 institutions across 4 countries. Total MTV (tMTV) was analyzed, with a 42% SUVmax threshold. Survival was analyzed according to high tMTV (≥ median). Plasma proteomic profile, whole exome, transcriptome and other analysis were performed on monocentric cohorts to explore its biological correlates.

Results:

Of the 518 patients included, 167 received ICBs, 257 had chemotherapy plus ICBs, and 94 had chemotherapy. Median tMTV was 99 cm^3. Median overall survival (OS) for patients with high tMTV treated with ICBs was 11.4 months vs 29.6 months (P<0.0012) for those with low tMTV. In patients receiving chemotherapy-ICB tMTV did not correlate with OS (P=0.099). In patients with PD-L1≥1% and high tMTV, chemotherapy-ICB combination was associated with longer OS compared with ICBs alone (20 vs 11.4 months,p=0.026), while no survival differences observed in low tMTV group. High tMTV correlated (and its detrimental effect seems to be driven by) a specific proteomic profile and increase in genomic instability.

Conclusion:

Our analysis indicates high tTMV is linked to an increase in systemic inflammation, specific cytokines production and chromosomal instability. tTMV may serve as one of the biomarker to select the best upfront strategy in patients with PD-L1 positive advanced NSCLC.

Introduction

Immune checkpoint blockers (ICBs) have revolutionized the treatment paradigm for non-small cell lung cancer (NSCLC). Nonetheless, while some patients experience significant and long-lasting disease regression with ICBs, a large proportion of the population does not benefit, and furthermore some patients may even experience the negative effect of hyperprogressive disease[1,2]. The programmed death-ligand 1 (PD-L1) tumor proportion score (TPS) assessed by immunohistochemistry is currently the most commonly used biomarker to predict outcomes of inhibitors of programmed cell death protein 1 (PD-1) and PD-L1[3]. However, as lack of sensitivity and specificity resides among the major limitations of PD-L1 quantification, it is not considered the definitive biomarker[4].

Predicting benefit before ICB initiation is becoming increasingly relevant with the advent of combination chemo-immunotherapy in the therapeutic envelope. For patients with high PD-L1 expression (≥ 50% in Europe, ≥ 1% in US) NSCLC, guidelines describe ICBs alone and in combination with chemotherapy as a first-line treatment option[5,6]. Both have proven superior to chemotherapy alone in phase 3 trials, with similar median overall survival (OS) and 3-year OS [7–9], however a head-to-head comparison, which is mandatory to assess their respective risk-benefit profiles, has not been performed. A recent Food and Drug Administration (FDA) meta-analysis suggested only a marginal benefit in progression-free survival (PFS) and no benefit in OS when ICBs were administered as combination therapy in the PD-L1-high patient population, highlighting the need for shared decision-making in balancing pros and cons with the patient on a case-by-case base[10].

Identification of biomarkers that are readily evaluable is crucial to enable feasible implementation in routine clinical practice. In addition to PD-L1, several other potential biomarkers have been proposed, among them lactate dehydrogenase (LDH) serum levels,

circulating DNA or tumor cells, white blood cell counts and ratio, T cell senescence, and the gut microbiome[11–14]. Many of these proposed biomarkers correlate with tumor burden, and increasing evidence supports a negative impact of tumor burden on the immune response to cancer [15].

18F-fluorodeoxyglucose 18F-FDG positron emission tomography (PET)-derived total metabolic tumor volume (tMTV) is a simple means to assess cancer lesions in vivo, thereby evaluating whole-body tumor burden. It has been shown to correlate with ICB outcome in melanoma[16,17], and more recently in NSCLC[18], however most evidence comes from small, single-center studies lacking a control group. Little is known about the biological changes that occur in the tumor microenvironment and host with increasing tMTV. This relationship may be explained by a larger tumor being the result of a deficit in the patient's immune-surveillance, thereby allowing the tumor to grow more quickly before being detected. This may be due to a different initial tumor biology presenting a higher proliferation rate and more aggressive behavior, or through dynamic changes occurring when tumors increase in size.

The aim of this retrospective study was to analyze the impact of tMTV in patients with advanced NSCLC treated with ICBs alone, with chemotherapy, or a combination of both, and investigate the effect of the addition of chemotherapy to ICBs in relation to tMTV. The study also explores biological correlates of tMTV that may explain its negative association with ICB efficacy, potentially opening avenues for new treatment strategies.

Methods

Patients

For analysis of tMTV as a biomarker, patients receiving first-line treatment for advanced NSCLC with an ICB, a combination of platinum-based chemotherapy and an ICB, or chemotherapy alone, were retrospectively identified from 11 institutions across 4 European countries. To be eligible, patients had to have undergone an 18F-FDG PET/computed tomography (CT) scan within 42 days before treatment initiation and, if alive at the time of inclusion, have at least 6 months of follow-up. Institutional ethics review board approval was obtained (IRB number 2021-13_18/01/2021). For analysis of biological correlates of tMTV, an independent cohort was analyzed including patients retrospectively identified from four prospective trials performed at the Gustave Roussy. Patients were included irrespective of the line (localized, first line and beyond) and type of treatment received (immunotherapy with or without chemotherapy); to be eligible, patients had to have advanced NSCLC, a PET/CT scan within 42 days before sampling for blood-based biomarkers or biopsy for genome and transcriptome analysis, and have not received anticancer treatment between the PET scan and sample collection, except for gut microbiota analysis where stool sampling before or after the PET/CT scan but within the same time window was allowed. Plasma proteomic analysis was performed with patients from the PREMIS (NCT02517892) and MATCH-R (NCT03984318) prospective studies, genome and transcriptome analyses were performed with patients from the MATCH-R and PRINCEPS (NCT02994576) studies, and gut microbiome analyses were performed with patients from the ONCOBIOTICS study (NCT04567446). All the studies were conducted in accordance with Declaration of Helsinki and informed consent was collected from each subject or each subject's guardian according to local regulations.

PET/CT scan analysis

18F-FDG PET/CT images were acquired 55-75 minutes post-injection. Respiratory-gated protocols were permitted provided that the local analysis was systematically performed using the same acquisition method. Patients were required to fast for at least 6 hours prior to a scan. Medication intake was not restricted other than oral anti-diabetic drugs which were stopped on the day of the scan. Injected 18F-FDG activity was optimized for body weight according to EANM guidelines [19].

A fixed 42% relative threshold of SUVmax was chosen among the different types of segmentation to allow a simple and accessible assessment that minimized observer dependency and because it is one of the most widely described, used and accessible in dedicated visualization software's for tumor segmentation in FDG PET images [20,21]. tMTV was calculated by adding all hypermetabolic lesions >1 cm^3 for each 18F-FDG PET/CT examination from vertex to mid-thigh.

Proteomic and blood-based analysis

Blood samples were obtained at baseline for ICBs ± chemotherapy and those within 42 days from PET scan were selected for the analysis. Routine blood analysis (complete blood count and differential, LDH, C reactive protein [CRP]) was performed a single laboratory (Gustave Roussy). Plasma samples were assessed using the Olink® Target 96 inflammation panel for the PREMIS study and with Olink® Explore 1536 library in the MATCH-R study (Olink Proteomics AB, Uppsala, Sweden) according to the manufacturer's instructions[22]. The final assay readout was presented as NPX values, which is an arbitrary unit on a log2-scale where a high value corresponds to higher protein expression. All assay validation data (detection limits, intra- and inter-assay precision data, etc.) are available on the manufacturer's website (www.olink.com). The final assay readouts were presented as NPX values, which is an

arbitrary unit on a log2-scale where higher values correspond to higher protein expression. All assay validation data (detection limits, intra- and inter-assay precision data, etc.) are available on the manufacturer's website (www.olink.com).

As plasma proteomic measurements were obtained from two studies, partial correlation coefficients between two plasma proteomic measurements were obtained after controlling for cohort (see Supplementary Methods).

To explore the correlation of plasma proteomics with tMTV, a univariate linear regression model was used, with tMTV as outcome and cytokines as independent variables for primary variable selection, to identify plasma inflammatory cytokines significantly associated with tMTV.

To further investigate the effect of the selected cytokines, a Lasso penalized regression model was trained on 70% of the observations with three-fold repeated cross-validation using the tidymodels packages and workflow.

A univariate Cox model for OS was used for primary variable selection to identify plasma inflammatory cytokines significantly associated with OS. A penalized Cox regression with three-fold cross validation was used to further investigate the effect of the selected cytokines.

DNA and RNA library preparation

DNA and RNA were extracted from tumor biopsy samples and matched whole-blood samples at baseline for ICBs ± chemotherapy using the AllPrep DNA/RNA Mini Kit (Qiagen). DNA samples underwent sequencing on both Illumina HiSeq 2000 and Illumina NovaSeq platforms as paired-end reads. RNA libraries, prepared using the TruSeq Stranded mRNA kit, were similarly sequenced on Illumina NextSeq 500 and Illumina NovaSeq platforms as paired-end reads, according to the manufacturer's instructions.

Mutation calling

FASTQ files were cleaned and trimmed using FastQC v0.11.8. Fastp v0.20 (RRID:SCR_016962), and aligned with the reference human genome GRCh37. The GATK bundle v4.1.8.1 was used for alignment and calling. Somatic point mutations and small indels were detected with Mutect2 implementing a panel created from normal samples. Mutations were annotated using VEP release 104.

Segmentation, copy-number calling, and genomic instability score

Per-patient paired tumor versus normal samples reads were mapped using BWA-MEM (v0.7.12, RRID:SCR_022192) to the GRCh37 human genome reference. A bin size of 50 nucleotides was used for coverage and normalization. Bivariate (L2R and BAF) data were segmented and ploidy and tumor cellularity were obtained using ASCAT v2.5.2 (RRID:SCR_016868). Allele-specific absolute copy number identification was performed using EaCoN v0.3.6 (https://github.com/gustaveroussy/EaCoN) on R v4.1.1.

A genomic instability score (GIS) was computed based on the sum of the absolute difference between each segment copy number and the sample estimated ploidy multiplied by segments length and reported to the reference genome length, as previously described[23].

Gene differential expression and enrichment analysis

Differential gene expression depending on tMTV was determined as follows. Genes with very low expression were filtered out using a minimum cutoff of two counts in 10% of samples. DESeq2 v1.34.0 was used to generate principal component analysis (PCA) plots to detect and filter out outliers and identify differentially expressed genes with respect to tMTV. False discovery rates (FDR) were computed using the Benjamini-Hochberg method and an FDR cutoff of 0.05 was applied. Using log-fold change ranked values from differentially expressed genes, we performed enrichment analyses using the clusterProfiler package (v4.2.2, RRID:SCR_016884) and gene sets from the Molecular Signatures Database (MSigDB) using an FDR of 0.05%. The immune cell composition of the tumor microenvironment was quantified using the CIBERSORT absolute deconvolution method from the immunedeconv package (v2.0.4). The total immune infiltrate score was calculated from the sum of the different immune cell absolute scores in the sample.

T-cell senescence

Blood immune phenotyping was performed on fresh whole blood samples by flow cytometry as previously described[13]. Senescent immune phenotype (SIP) was measured as a percentage of $CD28^-$ $CD57^+$ $KLRG1^+$ among $CD8^+$ circulating lymphocytes. We considered SIP % both as a categorical variable (with the previously established cutoff of 39.5%[13]) and as a continuous variable, to explore the relationship with tMTV.

Intestinal microbiota

Fecal samples were prospectively collected from patients in the ONCOBIOTICS study following the International Human Microbiome Standards (IHMS) guidelines. For the scope of this analysis, only the timepoint within 42 days before or after a PET scan was considered, and maximum one dose of an ICB alone or in combination between the PET scan and sample collection was allowed. For metagenomic analysis, stools were processed for total DNA extraction and sequencing with Ion Proton technology following MetaGenoPolis (INRA) France, as previously reported[27]. The taxonomic profiling and quantification of microbial relative abundances of all metagenomic samples were done using MetaPhlAn 4.0 (RRID:SCR_004915) with default parameters. Bioinformatic analysis was performed with Python v3.8.2 or R v4.1.2.

Following MetaPhlAn 4.0 pipeline analysis, to enhance data robustness, only microbial species with a prevalence ≥20% were considered. Microbial relative abundances underwent transformations, normalization, and standardization using Sci-Kit learn package v1.0.1. Normalization and standardization processes ensured valid comparisons across species with different dynamic ranges. Microbiota diversity was assessed using the Richness and Shannon index for α diversity and Bray-Curtis dissimilarity for β-diversity. Principal coordinate analyses (PCoA) represented the exploratory analysis of β-diversity. Significance of data clustering for high and low tMTV was assessed using analysis of similarities (ANOSIM), calculated after 999 permutations. PCoA datapoints were color-coded with normalized and standardized classificatory variable values, providing Pearson ρ coefficient and *P* values. Partial least-squares discriminant analysis (PLS-DA) and variable importance plots (VIPs) identified discriminant microbial species. Bar thickness indicated fold ratio values for species' mean relative abundances between cohorts. Significance tests included Mann-

Whitney U and Kruskal-Wallis tests, with *P* values ≤ 0.05 considered significant. *P* values were corrected for multiple hypothesis testing using a two-stage Benjamini-Hochberg FDR at 10%. Receiver operating characteristic (ROC) analysis employed a machine learning model with a random forest classifier in Sci-Kit learn package v1.0.1, with default parameters. The analyses were conducted using Python v3.8.2 or R v4.1.2.

Statistical analysis

Descriptive statistics were used for the distribution of variables in the population. Predictors of PFS and OS were analyzed using univariate and multivariable Cox models. Penalized smoothing splines approach was used to assess linearity in a multivariable Cox model. Log transformation was applied for non-normally distributed variables. PFS and OS curves were estimated using the Kaplan-Meier method. Median follow-up was calculated with the reverse Kaplan-Meier method. Comparisons between subgroups were performed using log-rank testing. Correlation between variables and tMTV was performed using Pearson or Spearman correlation as appropriate.

Data availability

Clinical data are available for access upon external requests. Applicants should contact the following email address ‘camilo.garcia@gustaveroussy.fr’ to request access to clinical and raw data, that will be granted upon reasonable request.
Data for transcriptomic profile have been deposited to the European Genome-phenome Archive under the accession number EGAD00001009684. Please refer to the forms and README file from https://github.com/gustaveroussy/MetaPRISM_Public/tree/master/data for instructions on how to access the data.

No specific code has been written for this paper.

Results

Patient Population

Of the 518 patients analyzed, 167 received ICB monotherapy, 257 received a combination of chemotherapy and ICB, and 94 were treated with chemotherapy alone (Table 1). The median tMTV across the entire patient cohort was 99 cm^3 (IQR 45-179), and did not significantly differ among treatment groups. Patients treated with ICBs alone were slightly older and had higher PD-L1 expression compared to the other groups. The median follow-up duration was 28.8 months (95% CI 25 – 34.6)for ICBs, 16.8 months (95% CI 15 – 19.5) for chemotherapy-ICBs, and 79 months (95% CI 47.4 - NR) for chemotherapy. Patients with higher Eastern Cooperative Oncology Group (ECOG) performance status (PS) had higher median tMTV (177 cm^3 for ECOG PS $\geq$ 2 vs 93 cm^3 for ECOG PS 0-1, $P < 0.0001$), as well as those with liver metastasis (157 vs 93 cm^3, $P < 0.0001$) or bone metastasis (114 vs 86 cm^3, $P = 0.0002$). tMTV also correlated with LDH levels (rho 0.28, $P < 0.001$), and with derived neutrophil to lymphocyte ratio (dNLR; rho 0.12, $P = 0.009$). No correlation was found between tMTV and PD-L1 expression ($P = 0.268$), nor between tMTV and the presence of common molecular alterations, including *KRAS*, *TP53*, and *STK11*.

Overall Survival

Median OS for patients treated with ICBs alone was 19.1 months (95% confidence interval [CI] 16.2 – 29.6). In terms of tMTV, median OS was 11.4 months (95% CI 8.4 – 19.1) for patients with high tMTV versus 29.6 months (95% CI 21.4 – NR) for patients with low

tMTV (P = 0.0012; Figure 1A). In a multivariate model including known prognostic variables (Table 2), tMTV remained independently associated with OS, along with ECOG PS 2 and LDH above the upper limit of normal (ULN).

Median OS for patients treated with chemotherapy-ICBs was 17.3 months (95% CI 13.7–24.9). Patients with high tMTV had a median OS of 16.5 months (95% CI 11.8 – NR) vs 21.2 months (95% CI 15.3 – NR; P = 0.099) for those with low tMTV (Figure 1B). tMTV did not correlate with OS in a multivariate model (P = 0.6).

Median OS in the chemotherapy-treated cohort was 9.3 months (95% CI 6.9 – 11.7). Patients with high tMTV had a median OS of 7.0 months (95% CI 4.9 – 11.7) vs 10.2 months for those with low tMTV (95% CI 7.0 – 14.5; P = 0.078; Figure 1C). The multivariate model also showed no correlation of tMTV with OS in the chemotherapy group (P = 0.2).

Non-linearity of the impact of tMTV in the multivariable Cox model was explored by plotting using penalized smoothing splines. The shape of the curves differed between patients treated with ICBs alone and those with ICBs in combination with chemotherapy, with the hazard ratio showing sustained rise as tMTV increased in patients treated with ICBs alone, whereas for patients receiving combination therapy, the hazard ratio did not change significantly with increasing tMTV (Supplementary Figure S1).

We also investigated OS outcomes with ICBs alone vs combination of chemotherapy-ICBs in patients with PD-L1-positive tumors according to tMTV. In patients with high tMTV treated with ICBs alone, median OS was 11.4 months (95% CI 8.4 – 19.1) vs 20.0 months (95% CI 17.2 – NR) with the combination (P = 0.026; Figure 2). A multivariate model showed that treatment with chemotherapy plus ICBs was associated with longer OS compared to ICBs alone (HR 0.45, 95% CI 0.24, 0.85, P = 0.014; Table 3), while no difference was seen in patients with low tMTV (Supplementary Table S2, Figure 2B).

A multivariate Cox model was set up including all patients treated with ICBs or chemotherapy plus ICBs, with an interaction term between tMTV and treatment type, and showed a significant difference of effect between ICBs and chemotherapy plus ICBs (P = 0.009).

Progression-free survival

Median PFS for patients receiving ICBs alone was 9.2 months (95% CI 6.0 – 14.7). Patients with high-tMTV had a median PFS of 3.3 months (95% CI 1.9 - 6.4) compared to those with low tMTV who had a median PFS of 15.6 months (95% CI 11.7 - 23.5; P < 0.001; Figure 1A). When adjusting for known prognostic factors, the tMTV (log transformed) remained a significant predictor of PFS in multivariate analysis, alongside LDH values above the ULN (Table 4). In patients receiving chemotherapy in combination with ICBs, median PFS was 7.7 months (95% CI 7.0 - 10.1). Patients with high tMTV had a median PFS of 6.5 months (95% CI 5.3 - 7.7) compared to those with low tMTV with a median PFS of 10.4 months (95% CI 8.4 - 14.2), with a significant difference observed (P = 0.023; Figure 1B). After adjusting for known prognostic biomarkers, tMTV correlated with PFS, along with PD-L1 expression and dNLR (Table 4). No correlation was found between PFS and tMTV in the chemotherapy group (P = 0.18; Figure 1C, Table 4).

We also investigated PFS in patients with PD-L1-positive tumors following treatment with ICBs alone versus the chemotherapy-ICB combination according to tMTV. In patients with high tMTV and PD-L1 ≥ 1%, median PFS was 3.3 months (95% CI 1.9 – 5.8) for ICBs versus 7.8 months (95% CI 5.5 – 13.6) for chemotherapy plus ICBs (P = 0.048, Figure 2A). No difference was seen in patients with low tMTV (P = 0.93). A multivariate model showed that treatment with chemotherapy plus ICBs was associated with longer PFS compared to

ICBs alone (HR 0.54, 95% CI 0.31 - 0.93, *P* = 0.026; Table 3), while no difference was seen in those with low tMTV (Supplementary Table S2, Figure 2B).

Circulating blood and plasma proteomics correlates of tMTV

In determining potential correlates of tMTV, the role of inflammation was explored in a prospective independent cohort of 77 patients with advanced NSCLC and available characterization of circulating white blood cells and plasma proteomics. The main clinicopathological characteristics of this cohort are summarized in Supplementary Table S1. The association between survival and tMTV was analyzed in this independent population. In patients treated with ICBs alone and after stratification for first line vs later lines of treatment, tMTV correlated with OS as a continuous variable (HR 1.5, 95% CI 1.1 – 2.0, *P* = 0.007, Supplementary Figure S2A). tMTV was directly correlated with neutrophil counts (rho 0.38, *P* < 0.0001), monocyte counts (rho 0.36, *P* = 0.0001), CRP (rho 0.36, *P* < 0.0001), and LDH (rho 0.52 *P* < 0.0001). At a plasma proteomic profile level, a significant direct correlation (after FDR correction) was found between tMTV and several cytokines including IL8, MCP3, CDPC1, LIF, CSF1, CCL23, IL18, TGF-alpha, and IL6 (Figure 3A and Supplementary Table S4).

A penalized linear model was setup and three-fold cross-validated, to identify the main correlates of tMTV in terms of cytokines. Our model showed that, with the increase in tMTV, an increase in plasmatic cytokine levels was seen, in order of importance, in IL8, LIF, CCL23, CSF1, MCP3, and TGF-alpha (Figure 3C). Most of these cytokines were correlated with decreased OS (Supplementary Table S4).

We then explored if the detrimental effect of tMTV on OS was dependent on these cytokines using a machine learning survival model. This showed that IL8, CSF1, IL1-alpha, and

SLAMF1 had the most prominent detrimental effect on survival, with tMTV having no impact after accounting for these cytokines (Figure 3D).

Finally, we examined whether the relationship between the increase in plasma cytokine concentration and tMTV was directly linked to tumor production. We therefore analyzed the correlation between cytokine gene expression and plasma concentrations, finding significant correlations only for CCL7 (rho 0.44, $P < 0.001$), CXCL9 (rho 0.32, $P = 0.009$), and CCL20 (rho 0.31, $P = 0.01$). After correction for tMTV (correlation between plasma levels/tMTV ratio and corresponding gene expression) a significant positive association was found for CXCL1 (rho 0.56, $P = 0.03$). Notably, we found no significant correlation for IL8 (a mild positive, non-significant correlation was seen, rho 0.18, $P = 0.13$, in line with previous reports) or for CSF1. This suggests that, at least for some of the cytokines identified, their correlation with tumor burden might be mediated by their production by other tissues rather than directly by the tumor (Figure 3E and 3F).

DNA and RNA sequencing

As previous evidence has shown a link between cancer-related inflammation and genomic instability[23,24], we hypothesized that, as tumors increase in size along with the associated accumulation of cell division cycles, genomic instability may increase[23,25].

We analyzed the MATCH-R cohort (n=31) and, to further explore this hypothesis that genomic instability increases in parallel with cancer growth, we also used a second cohort of untreated, non-metastatic patients from the PRINCEPS phase 2 trial (n = 23).

Overall, a significant correlation between tMTV and genomic instability was seen (rho 0.52, $P = 0.0001$, Figure 4A). This was consistent across cohorts (MATCH-R rho = 0.38, $P = 0.038$) and for PRINCEPS (rho = 0.54, $P = 0.018$). Median GIS was higher in patients with

advanced disease (MATCH-R) than for those with localized disease (PRINCEPS; 0.68 vs 0.40, $P = 0.003$).

Differential expression analysis identified 568 genes differentially expressed with tMTV (Figure 4B). Enrichment analysis showed activation of gene ontology biological processes (GOBP) related to metabolism and inflammation with increasing tMTV (Figure 4C). We also found a negative correlation between tMTV and total immune cell contents (rho -0.57, $P < 0.0001$, Figure 4D).

RNA sequencing

Differential expression analysis identified 568 differentially expressed genes according to tMTV (Figure 4A). Enrichment analysis showed that different gene ontology biological process (GOBP) pathways were increasingly activated with increasing MTV (Figure 4B), in particular associated with metabolism and inflammation. We also found a negative correlation between tMTV and sum of immune cell scores (rho -0.57, $P < 0.0001$, Figure 4C).

Immune senescence and microbiota

Patients with available stool samples (n=61) were divided into two groups according to the median tMTV of this cohort (74 cm^3: 34 patients with low tMTV, versus 27 patients with high tMTV). No difference was seen in alfa- and beta diversity between the two categories of tMTV (Figure S3A-B). Normalized and standardized tMTV values were then used as a continuous variable to color data points in the PCoA ordination plot. This approach did not reveal significant results after Pearson correlation, along the x-axis ($\rho = 0.015$, $P = 0.911$) and y axis ($\rho = -0.120$, $P = 0.360$) (Supplementary Figure S3C). To assess the contribution of each microbial species to describe high or low tMTV categories, we employed PLS-DA. Out of

the top 50 species, 17 showed significant differences between high and low tMTV before FDR correction (Figure S3D), while none remained significant after FDR correction. Despite these apparently discouraging results, the StratifiedKFold random forest ROC curve, measuring the performance of pooling the relative abundances of these 17 selected MGS to predict patients as high or low tMTV, demonstrated promising results with an averaged AUC value of 0.745, a specificity of 0.828, and a sensitivity of 0.640 (Supplementary Figure S3E).

No correlation was found between immune senescence and tMTV, with immune senescence considered as categorical variable using the previously established 39.5% cutoff (median tMTV for SIP-positive 65.5 cm^3 vs 87.1 cm^3 for SIP-negative patients, $P = 0.6$) or as continuous variable ($P = 0.9$), Supplementary Figure S3F and S3G.

Discussion

In this large multicentric retrospective study, we demonstrated that in patients with advanced NSCLC, a high tMTV had a significant negative impact on the outcome of first line ICBs as monotherapy, both in terms of OS and PFS, and that intensification of this immunotherapy by combining it with chemotherapy improved the outcome of patients with high tMTV, whereas there was no beneficial effect in patients with low tMTV.

While the prognostic value of tMTV in patients receiving immunotherapy is in line with published evidence from smaller studies involving different cancer types[15], nonetheless, no data were available about its role in decision making in the context of intensification or deintensification of the treatment. With the observed limited impact of tMTV on treatment outcome, when chemotherapy was added to ICBs, we recommend that the combination be progressively preferred with increasing tMTV.

Our study further investigated this outcome by exploring the biological mechanisms underlying the impact of tMTV on immunotherapy outcome. After observing a correlation of tMTV with basic inflammatory markers such as dNLR, CRP and LDH, we further investigated the proteomic profile, finding that tMTV levels correlated with a series of cytokines involved in inflammation, immune cell recruitment and activation, immune regulation, cell proliferation and differentiation, tumor growth and metastasis, and immune cell communication and activation. Particularly intriguing is that the effect of tMTV on survival may be mediated by some of these cytokines, notably IL8. These findings support the notion that cancer can induce modifications in plasma that are dependent on its size. This may result from the direct secretion of proteins or may be mediated (in the case of IL-8, for example, it could be mediated by other cells in the tumor microenvironment[26]). This proteomic profile is associated with a reduced immune response.

This could explain the benefit observed with an intensification strategy. As the chemo-immunotherapy combination has a higher response rate than ICB monotherapy[7–9], it could lead to tumor shrinkage, resulting in the reduction of plasma levels of certain cytokines that, in turn, could help restore the immune response against cancer. This is particularly promising as new treatments with potentially higher response rate become available (eg, KRAS tyrosine kinase inhibitors) that could further increase the benefit in combinations with immunotherapy for patients with a high tumor burden.

Two other hypotheses for the mechanism of action were explored. First, that a higher tumor burden could be the result of impaired immune surveillance, a setting that could explain the reduced efficacy of ICBs on an already impaired immune system. To address this, we focused on T-cell senescence [27,28] and gut microbiota [2930], two biomarkers that are correlated with immune fitness, and found no correlation with tMTV. Then, we explored the hypothesis that higher tumor burden was the result of a different biology ab initio, at the genomic level, but we also did not find molecular alterations characterizing larger versus smaller tumors. We found instead that an increase in tMTV was linked to an increase in genomic instability, both in localized and in advanced disease. Genomic instability has been considered as a mechanism of immune escape and described as correlated with systemic inflammation, with available evidences supporting a two-sided relationship[23,24]. Moreover, at the transcriptome level, we found that an increase in tMTV was accompanied by higher activity in pathways linked to metabolism and inflammation, further reinforcing the link between tumor burden and inflammation.

Taken together, the current evidence from our study suggests that as tMTV increases, tumors become increasingly resistant to ICBs when administered as monotherapy. This seems to be mediated at least in part by cytokines directly released or indirectly induced by the tumor,

and proportionally to the tumor mass, as well as by accumulated genomic instability. This reinforces the use of an intensified regime combining chemotherapy and immunotherapy to reduce tumor burden and potentially increase immunotherapy efficacy. This finding also contradicts the idea that a higher tMTV is the result of an already impaired immune system or a different tumor biology from the outset.

Among the strengths of our study were the number of participating patients and centers, which allow a higher generalizability, the presence of intensified and de-intensified immunotherapy-based regimen, as well as the use of proteomic, DNA, and RNA biomarker data in an independent cohort to explore the biological mechanisms behind tMTV. Limitations of this study include the retrospective design. Also, PET scans are not systematically done at diagnosis in this population, leading to possible biases in center selection. However, the large sample size goes some way towards balancing these limitations. Similarly, in the three independent cohorts analyzed for the biological correlates of tMTV, PET scans were not systematically performed at sample collection which could have impacted these results (for example, the relatively low number of patients with stool collection for microbiota), albeit the prospective nature of the three studies with stringent inclusion criteria reduces the risk of selecting a non-representative subgroup.

Conclusion and perspectives

Our data confirm that high tMTV, a surrogate biomarker of tumor burden, is associated with a low probability of benefiting from ICB monotherapy, whereas this prognostic value is mitigated by the addition of chemotherapy. Higher tMTV is correlated with a specific signal in plasma proteomics , which accounts for most of the impact on the immune response to the tumor, and with genomic instability. In the case of PD-L1-positive patients, a combination approach that includes chemotherapy along with ICBs may be a better choice when tMTV is

high. Further research is needed to fully understand the relationship between tumor burden, measured by tMTV or other innovative techniques, such as ctDNA measures, and the immune system.

References

1. Ferrara, R. *et al.* Hyperprogressive Disease in Patients With Advanced Non–Small Cell Lung Cancer Treated With PD-1/PD-L1 Inhibitors or With Single-Agent Chemotherapy. *JAMA Oncol.* (2018). doi:10.1001/jamaoncol.2018.3676
2. Kim, C. G. *et al.* Hyperprogressive disease during PD-1/PD-L1 blockade in patients with non-small-cell lung cancer. *Ann. Oncol.* **30**, 1104–1113 (2019).
3. Ott, P. A. *et al.* T-cell–inflamed gene-expression profile, programmed death ligand 1 expression, and tumor mutational burden predict efficacy in patients treated with pembrolizumab across 20 cancers: KEYNOTE-028. *J. Clin. Oncol.* **37**, 318–327 (2019).
4. Davis, A. A. & Patel, V. G. The role of PD-L1 expression as a predictive biomarker: an analysis of all US Food and Drug Administration (FDA) approvals of immune checkpoint inhibitors. *J. Immunother. Cancer* **7**, 278 (2019).
5. Hendriks, L. E. *et al.* Non-oncogene-addicted metastatic non-small-cell lung cancer: ESMO Clinical Practice Guideline for diagnosis, treatment and follow-up. *Ann. Oncol.* **34**, 358–376 (2023).
6. Jaiyesimi, I. A. *et al.* Therapy for Stage IV Non–Small Cell Lung Cancer Without Driver Alterations: ASCO Living Guideline, Version 2023.3. *J. Clin. Oncol.* **42**, e23–e43 (2024).
7. Reck, M. *et al.* Pembrolizumab versus Chemotherapy for PD-L1–Positive Non–Small-Cell Lung Cancer. *N. Engl. J. Med.* **375**, 1823–1833 (2016).
8. Gandhi, L. *et al.* Pembrolizumab plus Chemotherapy in Metastatic Non–Small-Cell Lung Cancer. *N. Engl. J. Med.* **378**, NEJMoa1801005 (2018).
9. Paz-Ares, L. *et al.* Pembrolizumab plus Chemotherapy for Squamous Non–Small-Cell Lung Cancer. *N. Engl. J. Med.* **379**, 2040–2051 (2018).

10. Akinboro, O. *et al.* Outcomes of anti–PD-(L)1 therapy with or without chemotherapy (chemo) for first-line (1L) treatment of advanced non–small cell lung cancer (NSCLC) with PD-L1 score ≥ 50%: FDA pooled analysis. *J. Clin. Oncol.* **40**, 9000–9000 (2022).
11. Reichert, Z. R. *et al.* Prognostic value of plasma circulating tumor DNA fraction across four common cancer types: a real-world outcomes study. *Ann. Oncol.* (2022). doi:10.1016/j.annonc.2022.09.163
12. Dall'Olio, F. G. *et al.* PD-L1 Expression in Circulating Tumor Cells as a Promising Prognostic Biomarker in Advanced Non–small-cell Lung Cancer Treated with Immune Checkpoint Inhibitors. *Clin. Lung Cancer* **22**, 423–431 (2021).
13. Ferrara, R. *et al.* Circulating T-cell Immunosenescence in Patients with Advanced Non–small Cell Lung Cancer Treated with Single-agent PD-1/PD-L1 Inhibitors or Platinum-based Chemotherapy. *Clin. Cancer Res.* (2020). doi:10.1158/1078-0432.CCR-20-1420
14. Derosa, L. *et al.* Intestinal Akkermansia muciniphila predicts clinical response to PD-1 blockade in patients with advanced non-small-cell lung cancer. *Nat. Med.* **28**, 315–324 (2022).
15. Dall'Olio, F. G. *et al.* Tumour burden and efficacy of immune-checkpoint inhibitors. *Nat. Rev. Clin. Oncol.* **19**, 75–90 (2022).
16. Seban, R. D. *et al.* Prognostic and theranostic 18F-FDG PET biomarkers for anti-PD1 immunotherapy in metastatic melanoma: association with outcome and transcriptomics. *Eur. J. Nucl. Med. Mol. Imaging* **46**, 2298–2310 (2019).
17. Seban, R. D. *et al.* Prognostic 18F-FDG PET biomarkers in metastatic mucosal and cutaneous melanoma treated with immune checkpoint inhibitors targeting PD-1 and CTLA-4. *Eur. J. Nucl. Med. Mol. Imaging* **47**, 2301–2312 (2020).
18. Dall'Olio, F. G. *et al.* Baseline total metabolic tumour volume on 2-deoxy-2-

[18F]fluoro-d-glucose positron emission tomography-computed tomography as a promising biomarker in patients with advanced non–small cell lung cancer treated with first-line pembrolizumab. *Eur. J. Cancer* **150**, 99–107 (2021).

19. Boellaard, R. *et al.* FDG PET/CT: EANM procedure guidelines for tumour imaging: version 2.0. *European Journal of Nuclear Medicine and Molecular Imaging* **42**, 328–354 (2015).
20. Im, H.-J., Bradshaw, T., Solaiyappan, M. & Cho, S. Y. Current Methods to Define Metabolic Tumor Volume in Positron Emission Tomography: Which One is Better? *Nucl. Med. Mol. Imaging (2010).* **52**, 5–15 (2018).
21. Erdi, Y. E. *et al.* Segmentation of lung lesion volume by adaptive positron emission tomography image thresholding. *Cancer* **80**, 2505–9 (1997).
22. Assarsson, E. *et al.* Homogenous 96-plex PEA immunoassay exhibiting high sensitivity, specificity, and excellent scalability. *PLoS One* **9**, e95192 (2014).
23. Danlos, F.-X. *et al.* Genomic Instability and Protumoral Inflammation Are Associated with Primary Resistance to Anti–PD-1 + Antiangiogenesis in Malignant Pleural Mesothelioma. *Cancer Discov.* **13**, 858–879 (2023).
24. Colotta, F., Allavena, P., Sica, A., Garlanda, C. & Mantovani, A. Cancer-related inflammation, the seventh hallmark of cancer: links to genetic instability. *Carcinogenesis* **30**, 1073–1081 (2009).
25. Li, J. *et al.* Non-cell-autonomous cancer progression from chromosomal instability. *Nature* **620**, 1080–1088 (2023).
26. Teijeira, A. *et al.* IL8, Neutrophils, and NETs in a Collusion against Cancer Immunity and Immunotherapy. *Clin. Cancer Res.* **27**, 2383–2393 (2021).
27. Zhang, J., He, T., Xue, L. & Guo, H. Senescent T cells: a potential biomarker and target for cancer therapy. *EBioMedicine* **68**, 103409 (2021).

28. Lian, J., Yue, Y., Yu, W. & Zhang, Y. Immunosenescence: a key player in cancer development. *J. Hematol. Oncol.* **13**, 151 (2020).

29. Zheng, D., Liwinski, T. & Elinav, E. Interaction between microbiota and immunity in health and disease. *Cell Res.* **30**, 492–506 (2020).

30. Zitvogel, L., Ayyoub, M., Routy, B. & Kroemer, G. Microbiome and Anticancer Immunosurveillance. *Cell* **165**, 276–287 (2016).

Tables and Figures

Table 1 – Clinicopathologic characteristics of the three cohorts of patients treated with immune checkpoint blockers alone, in combination with chemotherapy, or with chemotherapy alone.

Characteristic	**Immune checkpoint blockers** N = 167[1]	**Chemotherapy + Immune checkpoint blockers** N = 257[1]	**Chemotherapy** N = 94[1]	***P* value**[2]
Sex				0.2
Male	113 (68%)	183 (71%)	58 (62%)	
Female	54 (32%)	74 (29%)	36 (38%)	
Bone Metastasis	70 (42%)	114 (44%)	45 (48%)	0.6
Liver Metastasis	26 (16%)	30 (12%)	21 (22%)	**0.043**
Brain Metastasis	32 (20%)	61 (24%)	25 (27%)	0.4
ECOG PS ≥ 2	29 (17%)	39 (15%)	17 (18%)	0.7
Age (years)	70 (61, 76)	64 (57, 71)	63 (55, 68)	**<0.001**
PD-L1				**<0.001**
TPS ≥50%	167 (100%)	58 (24%)	2 (11%)	
TPS 1 – 49%	0 (0%)	89 (36%)	5 (26%)	
TPS <1%	0 (0%)	99 (40%)	12 (63%)	
Unknown	0	11	75	
LDH > ULN	46 (35%)	83 (38%)	29 (33%)	0.7
Unknown	35	39	7	
Chemotherapy regimen				
Cisplatin		67 (26%)	57 (61%)	

Carboplatin		190 (74%)	37 (39%)	
None	167	0	0	
Histological type				0.5
Adenocarcinoma	120 (72%)	188 (73%)	66 (70%)	
Squamous cell	32 (19%)	46 (18%)	14 (15%)	
Other/NOS	15 (9.0%)	23 (8.9%)	14 (15%)	
Total tMTV (cm^3)	93 (43, 164)	101 (44, 185)	97 (50, 181)	0.5

[1] n (%); Median (IQR)

[2] Pearson's Chi-squared test; Kruskal-Wallis rank sum test

Abbreviations: ECOG PS: Eastern Cooperative Oncology Group performance status; LDH: lactate dehydrogenase; MTV: metabolic tumor volume; NOS: not otherwise specified; PD-L1: programmed death-ligand 1; TPS: tumor proportion score. ULN: upper limit of normal.

Table 2 – Multivariate model for overall survival in patients receiving immune checkpoint blockers alone, immune checkpoint blockers in combination with chemotherapy, or chemotherapy alone.

	Immune checkpoint blockers			**Chemotherapy plus immune checkpoint blockers**			**Chemotherapy**		
Characteristic	**HR**[1]	**95% CI**[1]	***P* value**	**HR**[1]	**95% CI**[1]	***P* value**	**HR**[1]	**95% CI**[1]	***P* value**
Log tMTV	1.53	1.12, 2.08	**0.007**	1.05	0.87, 1.27	0.6	1.20	0.92, 1.56	0.2
Bone metastasis (yes vs no)	1.56	0.92, 2.63	0.10	1.26	0.83, 1.91	0.3	0.79	0.50, 1.26	0.3
Liver metastasis (yes vs no)	0.85	0.44, 1.64	0.6	1.60	0.87, 2.95	0.13	1.04	0.58, 1.85	>0.9
Brain metastasis (yes vs no)	0.65	0.32, 1.35	0.2	0.98	0.61, 1.59	>0.9	1.10	0.65, 1.84	0.7
ECOG PS (≥ 2 vs 0-1)	1.99	1.07, 3.69	**0.029**	1.36	0.77, 2.39	0.3	2.10	1.05, 4.19	**0.036**
LDH (> ULN vs < ULN)	1.74	1.02, 2.96	**0.041**	1.07	0.68, 1.67	0.8	1.69	0.99, 2.87	0.053
dNLR (> 3 vs < 3)	1.50	0.90, 2.48	0.12	1.71	1.13, 2.58	**0.011**	1.23	0.75, 2.00	0.4
PD-L1 TPS	0.32	0.06, 1.63	0.2	0.44	0.21, 0.92	**0.029**			

[1] HR = hazard ratio, CI = confidence interval

Abbreviations: dNLR: derived neutrophil to lymphocyte ratio; ECOG PS: Eastern Cooperative Oncology Group performance status; LDH: lactate dehydrogenase; PD-L1: programmed death l ligand 1; PD-L1: programmed death-ligand 1; tMTV: total metabolic tumor volume; TPS: tumor proportion score; ULN: upper limit of normal.

Table 3 – Multivariate model for overall survival and progression-free survival in patients with high total metabolic tumor volume and PD-L1 tumor proportion score ≥ 1%

	OS			PFS		
Characteristic	**HR[1]**	**95% CI[1]**	**p-value**	**HR[1]**	**95% CI[1]**	**p-value**
Treatment (CT-ICBs vs ICBs)	0.45	0.24, 0.85	**0.014**	0.54	0.31, 0.93	**0.026**
Bone metastasis (yes vs no)	1.32	0.76, 2.28	0.3	1.27	0.78, 2.09	0.3
Liver metastasis (yes vs no)	0.97	0.51, 1.85	>0.9	1.09	0.61, 1.95	0.8
LDH > ULN (yes vs no)	1.54	0.87, 2.71	0.14	1.37	0.83, 2.26	0.2
ECOG PS ≥ 2 (yes vs no)	2.19	1.23, 3.91	**0.008**	1.90	1.13, 3.22	**0.016**
dNLR ≥ 3 (yes vs no)	1.97	1.14, 3.39	**0.014**	1.85	1.14, 3.01	**0.013**
PD-L1 TPS	0.74	0.21, 2.52	0.6	0.52	0.18, 1.45	0.2
Brain metastasis (yes vs no)	0.88	0.47, 1.66	0.7	0.83	0.47, 1.45	0.5

[1] HR = hazard ratio, CI = confidence interval
Abbreviations: CT-ICBs: chemotherapy plus immune checkpoint blockers; dNLR: derived neutrophil to lymphocyte ratio; ICB: immune checkpoint blockers; ECOG PS: Eastern Cooperative Oncology Group performance status; TPS: tumor proportion score; ULN: upper limit of normal.

Table 4 – Multivariate model for progression-free survival in immune checkpoint blockers alone, immune checkpoint blockers in combination with chemotherapy, or chemotherapy alone.

	Immune checkpoint blockers			**Chemotherapy plus immune checkpoint blockers**			**Chemotherapy**		
Characteristic	**HR**[1]	**95% CI**[1]	**p-value**	**HR**[1]	**95% CI**[1]	**p-value**	**HR**[1]	**95% CI**[1]	**p-value**
Log tMTV	1.34	1.03, 1.73	**0.029**	1.21	1.03, 1.42	**0.023**	1.09	0.85, 1.40	0.5
Bone metastasis (yes vs no)	1.21	0.75, 1.96	0.4	1.23	0.87, 1.75	0.2	0.76	0.47, 1.22	0.3
Liver metastasis (yes vs no)	1.11	0.60, 2.06	0.7	1.55	0.91, 2.64	0.11	0.89	0.50, 1.57	0.7
Brain metastasis (yes vs no)	1.13	0.66, 1.93	0.7	0.92	0.61, 1.39	0.7	0.97	0.57, 1.66	>0.9
ECOG PS (≥ 2 vs 0-1)	1.65	0.94, 2.89	0.082	1.29	0.80, 2.08	0.3	2.15	1.11, 4.15	**0.023**
LDH (> ULN vs ≤ ULN)	1.73	1.09, 2.76	**0.020**	0.82	0.56, 1.19	0.3	1.73	1.01, 2.94	**0.045**
dNLR (≥ 3 vs < 3)	1.36	0.87, 2.14	0.2	1.67	1.18, 2.36	**0.004**	1.33	0.82, 2.14	0.2
PD-L1 TPS	0.62	0.14, 2.64	0.5	0.40	0.22, 0.72	**0.002**	-	-	-

[1] HR = hazard ratio, CI = confidence interval

Abbreviations: ECOG PS: Eastern Cooperative Oncology Group Performance Status; dNLR: derived neutrophil to lymphocyte ratio; LDH: lactate dehydrogenase; TPS: tumor proportion score; tMTV: total metabolic tumor volume.

Figure legends

Figure 1. Kaplan-Meier curves for overall survival (left) and progression-free survival (right) according to total metabolic tumor volume (tMTV) above (high) or below (low) the median for patients treated with immune checkpoint alone (a), immune checkpoint blockers plus chemotherapy (b), or chemotherapy (c). Dotted lines indicate confidence intervals.

Figure 2 - Overall survival (left) and progression free-survival (right) for immune checkpoint blockers (ICBs) vs chemotherapy plus ICBs (CT-ICBs) in patients with PD-L1 ≥1% according to high tMTV (a) and low tMTV (b). Dotted lines indicate confidence intervals.

Figure 3. Circulating blood and plasma proteomics correlates of tMTV in the proteomic analysis population of the MATCH-R and PREMIS studies. Volcano plot showing the plasma proteome profile associated with total metabolic tumor volume (tMTV) (a). Volcano plot showing the plasma proteome profile associated with overall survival (OS) (b). Path of Lasso regression coefficients according to lambda penalty showing the robust positive effect of plasma IL8 on tMTV with all coefficients converging toward zero as the penalty parameter increases, IL8 is the last variable coefficient to converge toward zero (c). Path of penalized Cox regression coefficients against to lambda penalty showing the effect of plasma IL8 on OS, all coefficients converge toward zero as the penalty parameter increases, IL8 is the last variable coefficient to converge toward zero (d). Heatmap showing Spearman correlation coefficients between gene expression in columns and plasmatic protein concentration in rows (e). Heatmap showing Spearman correlation coefficients between gene expression in columns and plasmatic protein concentration ratio on tMTV in rows to account for the effect of tMTV on plasma cytokines (f).

Figure 4. Molecular correlates of total metabolic tumor volume (tMTV). Correlation between genomic instability and tMTV in advanced NSCLC (MATCH-R cohort) and in localized NSCLC (PRINCEPS cohort) (a). Volcano plot with differentially expressed genes according to tMTV (b). Gene ontology pathways (GOPD) suppressed or activated with increasing tMTV. The size of the circle depends on the number of genes found in the pathway, and the colors vary depending on the statistical significance (c). Scatter plot of the sum of immune cells with CIBERSORT and tMTV (d).

Figure 1

a

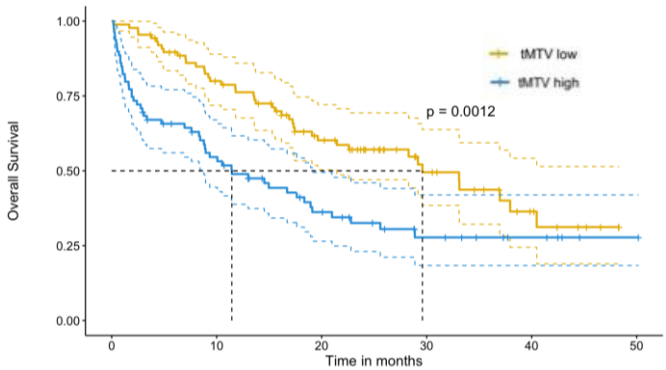

Number at risk: n (%)

tMTV low	88 (100)	65 (74)	41 (47)	19 (22)	8 (9)	0 (0)
tMTV high	79 (100)	39 (49)	22 (28)	10 (13)	5 (6)	1 (1)

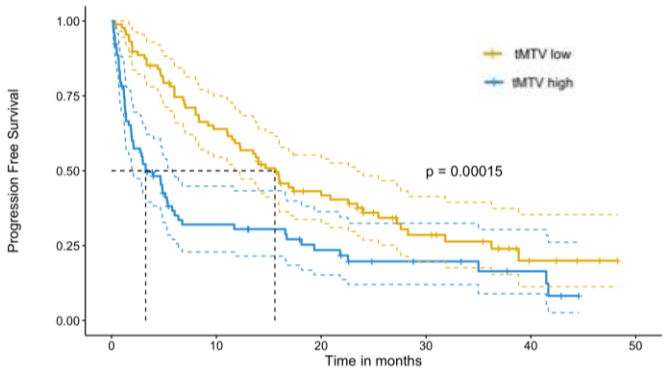

Number at risk: n (%)

tMTV low	88 (100)	54 (61)	31 (35)	15 (17)	4 (5)	0 (0)
tMTV high	79 (100)	21 (27)	13 (16)	7 (9)	4 (5)	0 (0)

b

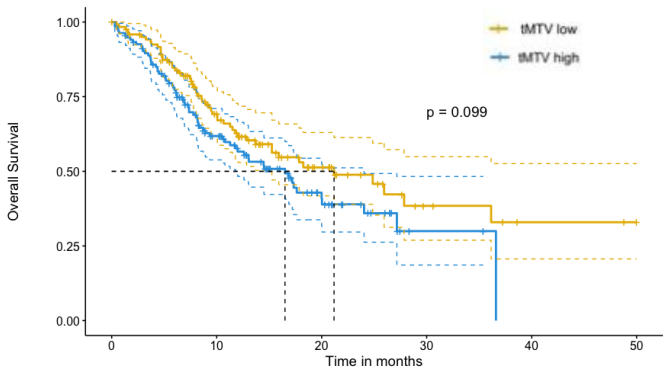

Number at risk: n (%)

tMTV low	122 (100)	66 (54)	26 (21)	8 (7)	4 (3)	3 (2)
tMTV high	135 (100)	64 (47)	21 (16)	2 (1)	0 (0)	0 (0)

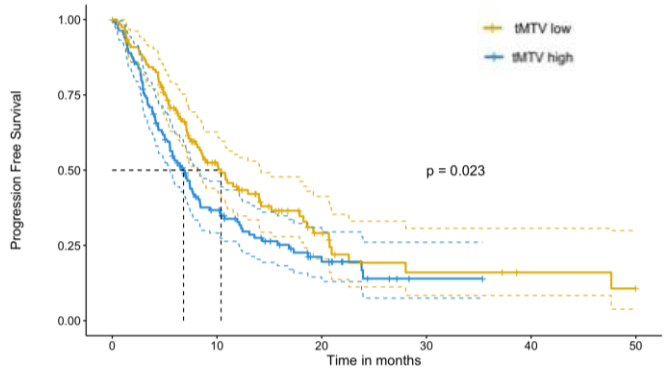

Number at risk: n (%)

tMTV low	122 (100)	47 (39)	14 (11)	5 (4)	3 (2)	2 (2)
tMTV high	135 (100)	40 (30)	12 (9)	1 (1)	0 (0)	0 (0)

c

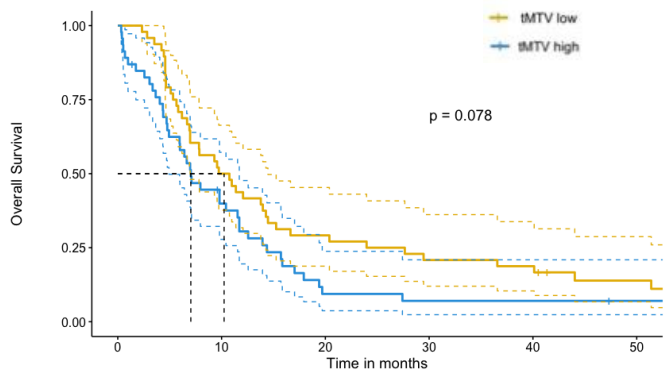

Number at risk: n (%)

tMTV low	48 (100)	24 (50)	14 (29)	10 (21)	9 (19)	5 (10)
tMTV high	46 (100)	17 (37)	4 (9)	3 (7)	3 (7)	2 (4)

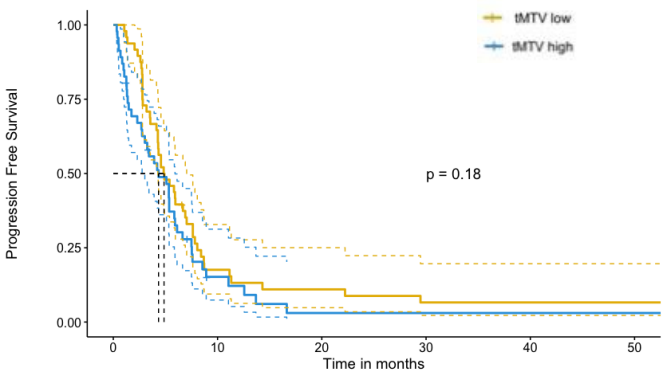

Number at risk: n (%)

tMTV low	48 (100)	8 (17)	5 (10)	3 (6)	3 (6)	3 (6)
tMTV high	46 (100)	5 (11)	1 (2)	1 (2)	1 (2)	1 (2)

Figure 2

a

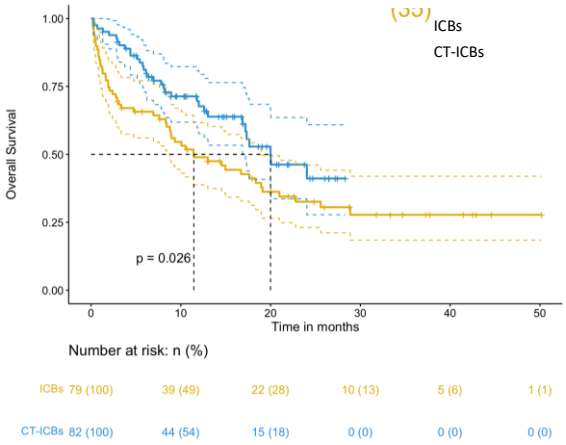
ICBs
CT-ICBs
Overall Survival
p = 0.026
Time in months
Number at risk: n (%)
ICBs 79 (100) 39 (49) 22 (28) 10 (13) 5 (6) 1 (1)
CT-ICBs 82 (100) 44 (54) 15 (18) 0 (0) 0 (0) 0 (0)

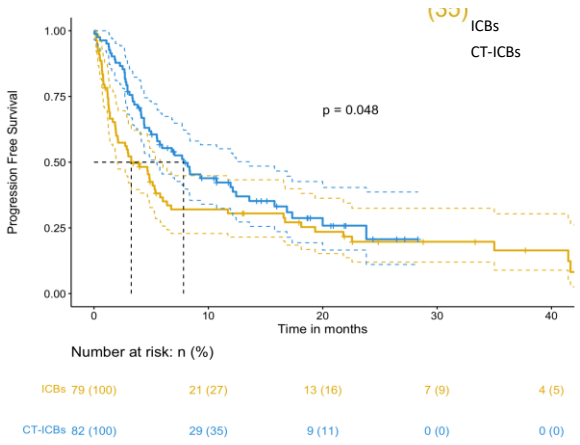
ICBs
CT-ICBs
Progression Free Survival
p = 0.048
Time in months
Number at risk: n (%)
ICBs 79 (100) 21 (27) 13 (16) 7 (9) 4 (5)
CT-ICBs 82 (100) 29 (35) 9 (11) 0 (0) 0 (0)

b

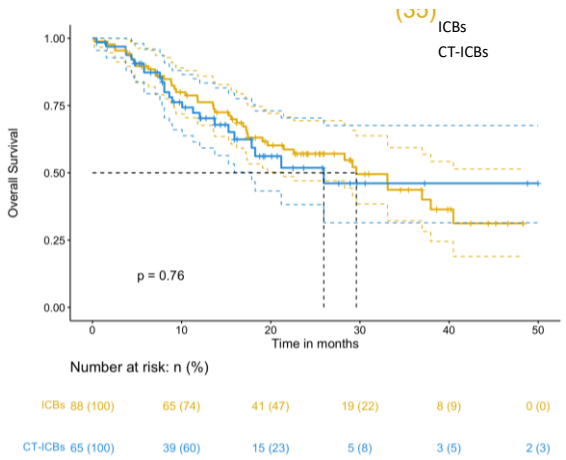
ICBs
CT-ICBs
Overall Survival
p = 0.76
Time in months
Number at risk: n (%)
ICBs 88 (100) 65 (74) 41 (47) 19 (22) 8 (9) 0 (0)
CT-ICBs 65 (100) 39 (60) 15 (23) 5 (8) 3 (5) 2 (3)

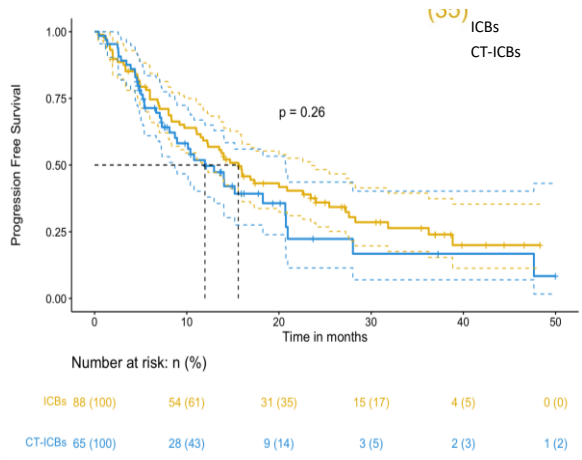
ICBs
CT-ICBs
Progression Free Survival
p = 0.26
Time in months
Number at risk: n (%)
ICBs 88 (100) 54 (61) 31 (35) 15 (17) 4 (5) 0 (0)
CT-ICBs 65 (100) 28 (43) 9 (14) 3 (5) 2 (3) 1 (2)

Figure 3

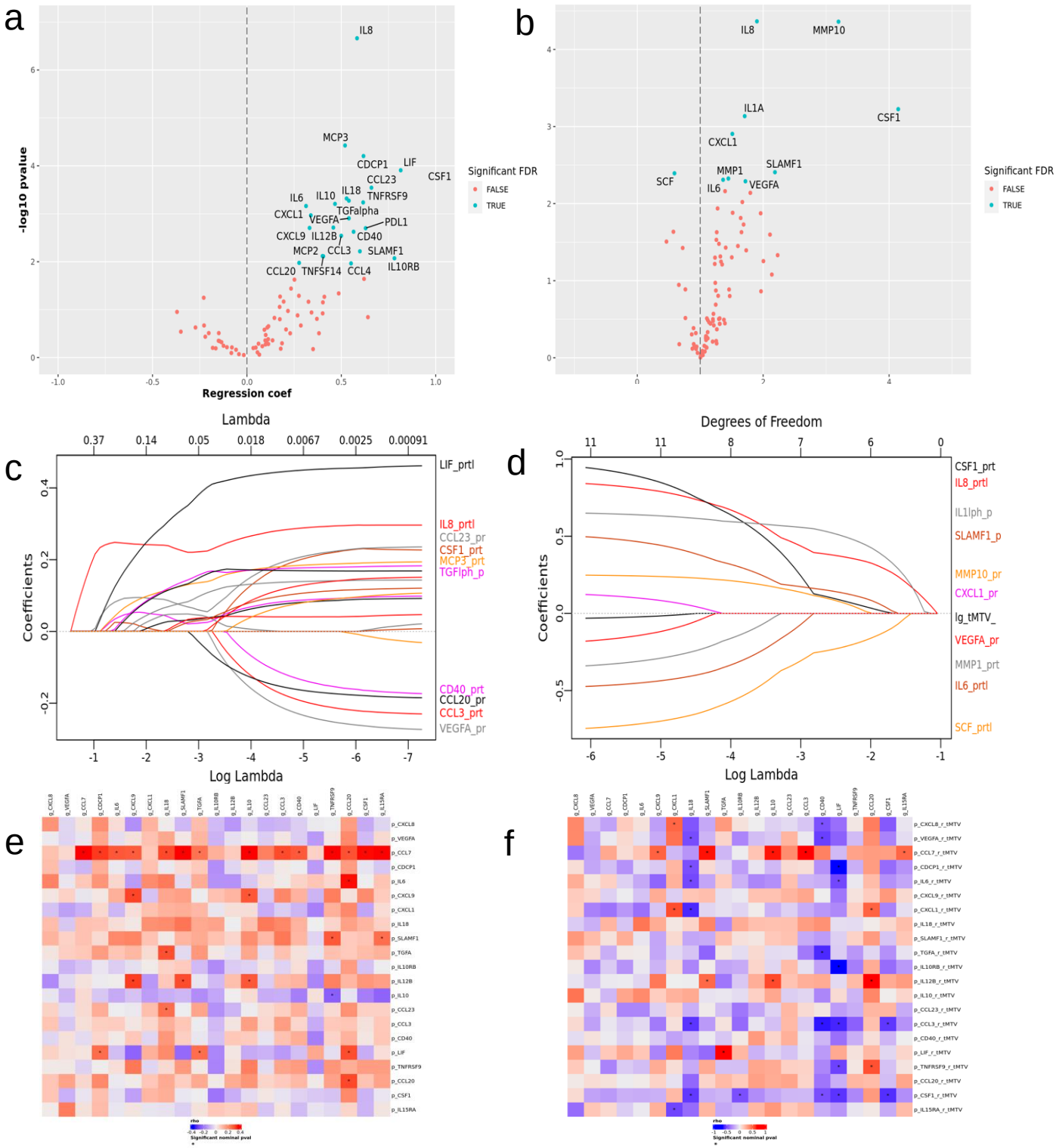
a
IL8
MCP3
CDCP1
LIF
CSF1
CCL23
IL6
IL10
IL18
TNFRSF9
CXCL1
VEGFA
TGFalpha
PDL1
CXCL9
IL12B
CD40
MCP2
CCL3
SLAMF1
CCL20
TNFSF14
CCL4
IL10RB
-log10 pvalue
Regression coef
Significant FDR
FALSE
TRUE
b
IL8
MMP10
IL1A
CSF1
CXCL1
SLAMF1
MMP1
SCF
IL6
VEGFA
Significant FDR
FALSE
TRUE
c
Lambda
0.37
0.14
0.05
0.018
0.0067
0.0025
0.00091
Coefficients
Log Lambda
LIF_prtl
IL8_prtl
CCL23_pr
CSF1_prt
MCP3_prt
TGFlph_p
CD40_prt
CCL20_pr
CCL3_prt
VEGFA_pr
d
Degrees of Freedom
11
11
8
7
6
0
Coefficients
Log Lambda
CSF1_prt
IL8_prtl
IL1lph_p
SLAMF1_p
MMP10_pr
CXCL1_pr
lg_tMTV_
VEGFA_pr
MMP1_prt
IL6_prtl
SCF_prtl
e
f
rho
Significant nominal pval

Figure 4

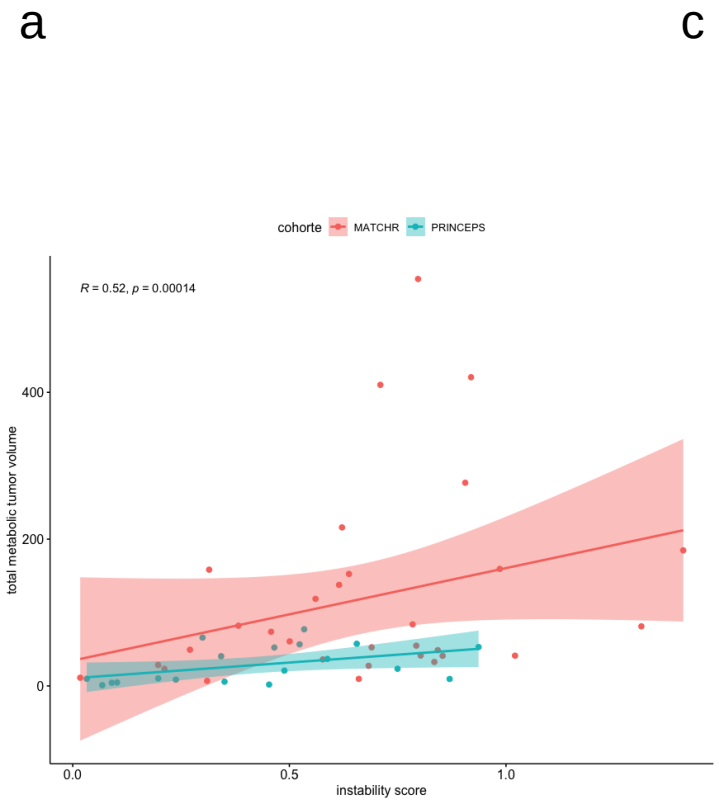
a
cohorte MATCHR PRINCEPS
R = 0.52, p = 0.00014
total metabolic tumor volume
instability score

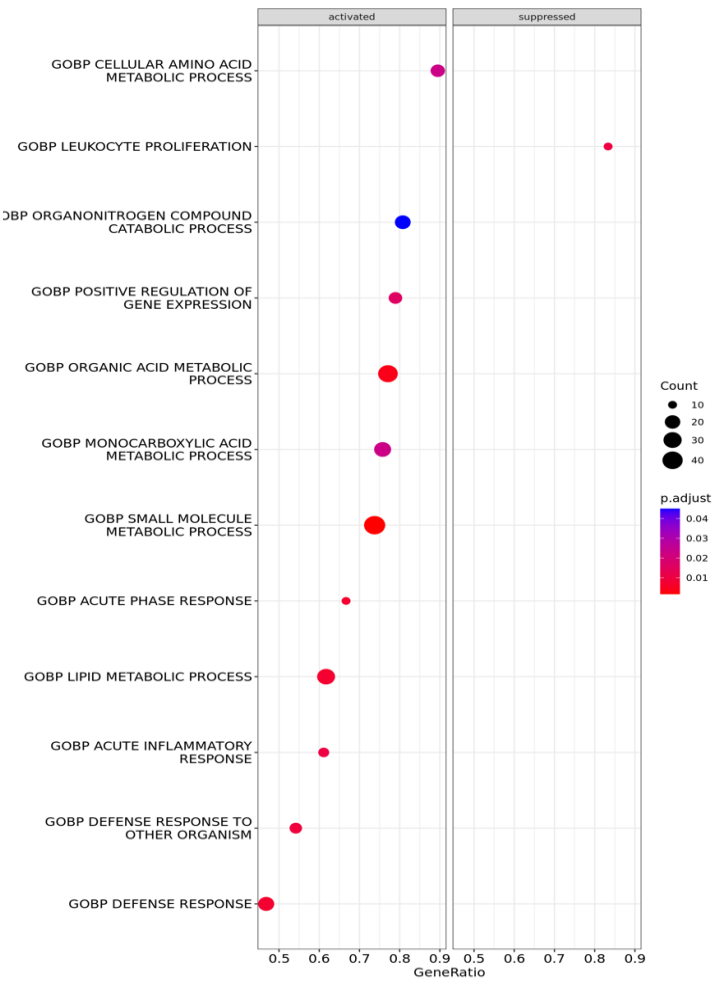
c
activated
suppressed
GOBP CELLULAR AMINO ACID METABOLIC PROCESS
GOBP LEUKOCYTE PROLIFERATION
GOBP ORGANONITROGEN COMPOUND CATABOLIC PROCESS
GOBP POSITIVE REGULATION OF GENE EXPRESSION
GOBP ORGANIC ACID METABOLIC PROCESS
GOBP MONOCARBOXYLIC ACID METABOLIC PROCESS
GOBP SMALL MOLECULE METABOLIC PROCESS
GOBP ACUTE PHASE RESPONSE
GOBP LIPID METABOLIC PROCESS
GOBP ACUTE INFLAMMATORY RESPONSE
GOBP DEFENSE RESPONSE TO OTHER ORGANISM
GOBP DEFENSE RESPONSE
Count
p.adjust
GeneRatio

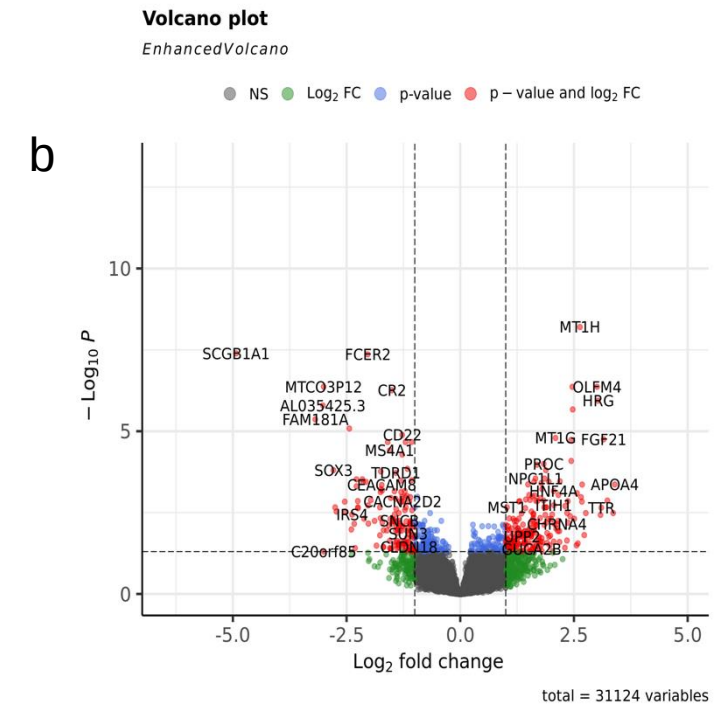
b
Volcano plot
EnhancedVolcano
NS Log2 FC p-value p – value and log2 FC
SCGB1A1
FCER2
MTCO3P12
CR2
AL035425.3
FAM181A
CD22
MS4A1
SOX3
TDRD1
CEACAM8
CACNA2D2
IRS4
SNCB
SUN3
C20orf85
CLDN18
MT1H
OLFM4
HRG
MT1G
FGF21
PROC
NPC1L1
HNF4A
APOA4
MST1
TEH1
TTR
CHRNA4
UPP2
GUCA2B
−Log10 P
Log2 fold change
total = 31124 variables

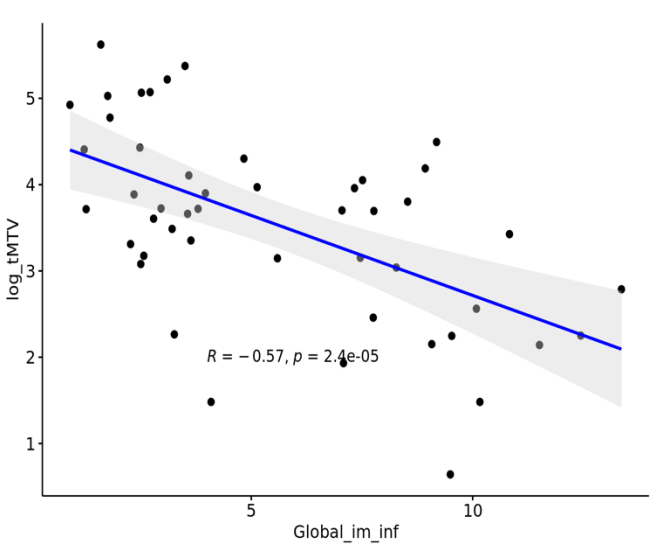
d
log_tMTV
R = −0.57, p = 2.4e-05
Global_im_inf